Magnetic properties and microstructure of FePt–Si_3N_4 nanocomposite thin films

Chih-Ming Kuo and P. C. Kuo[a)]
Institute of Materials Science and Engineering, National Taiwan University, Taipei, Taiwan

(Received 5 March 1999; accepted for publication 24 September 1999)

$(Fe_{50}Pt_{50})_{100-x}$–$(Si_3N_4)_x$ ($x=0-50$ vol. %) nanocomposite thin films are prepared by dc and rf magnetron cosputtering of FePt and Si_3N_4 targets on silicon wafer substrates, then annealed in vacuum at various temperatures. The effects of Si_3N_4 volume fraction, film thickness, and annealing temperatures on the magnetic properties are investigated. Transmission electron microscopy analysis indicated that structurally the film is an amorphous Si_3N_4 matrix with spherical FePt particles dispersed in it. The particle size of FePt increases with the annealing temperature but decreases with increasing Si_3N_4 content. Magnetization measurements indicated that maximum in-plane squareness and coercivity occurs at 30 vol. % of Si_3N_4 after annealing the film at 750 °C for 30 min. The average particle size of FePt in this film is about 40 nm. Saturation magnetization of the FePt–Si_3N_4 film is independent of film thickness but inversely proportional to the Si_3N_4 volume fraction. Variation of the films' coercivity with film thickness is small. In contrast, the magnetic hardening mechanism and coercivity of the FePt–Si_3N_4 composite film are dependent on the Si_3N_4 volume fraction. © *2000 American Institute of Physics.* [S0021-8979(00)05501-8]

I. INTRODUCTION

Since long ago, the most important problem in magnetic recording medium has been how to increase its recording density. A high recording density thin film medium needs high coercivity *Hc* and optimum remnant magnetization *Mr* for giant magnetic resistance (GMR) and MR read heads. At present, the CoCrM (M=Ni, Ta, Pt) crystalline thin films and columnar grain CoCr films are the most widely used longitudinal and perpendicular magnetic recording materials, respectively, due to their high coercivity. For these metallic films, the most significant problem is the noise that results from magnetic exchange coupling between the grains.[1] The key point for reducing media noise is the reduction of the intergrain magnetostatic and exchange interaction. Therefore, composite granular films with isolated magnetic grains dispersed in a nonmagnetic matrix are expected to become more suitable for high-density magnetic recording media over 10 Gb/in.[2] in the future due to their low noise characteristics.

Magnetic granular thin films having a kind of special structure usually consist of nanoscale ferromagnetic particles (e.g., Fe, Co, Ni, CoPt, etc.) which are embedded in an insulator matrix (e.g., SiO_2, Si_3N_4, Al_2O_3, etc.).[2–5] The magnetic properties of granular thin film are different than that of continuous metal thin films due to the magnetic particles of granular film being isolated. Furthermore, the growth of magnetic particles is constricted by a nonmagnetic matrix during heat treatment. The change in nonmagnetic matrix volume fraction changes the magnetic particles' intergranular distance, average grain size, and particle shape. These parameters all directly affect the magnetic properties of granular thin film. The particle size of magnetic particles in the film is much more easily controlled by process parameters than those in continuous metal film. Additionally, granular media have many better properties such as oxidation resistance, corrosion resistance, and wear resistance due to the magnetic particles being surrounded by an insulating matrix.

FePt is suitable for the magnetic material of granular media due to its high magnetocrystalline anisotropy ($K_u \cong 7\times10^7$ erg/cm^3).[6] In this article, we have fabricated granular FePt–Si_3N_4 thin films and investigated the effects of Si_3N_4 volume fraction, film thickness, and annealing temperature on the magnetic properties parallel and normal to the film plane.

II. EXPERIMENT

$(Fe_{50}Pt_{50})_{100-x}$–$(Si_3N_4)_x$ ($x=0-50$ vol. %) composite films with thicknesses of 10–200 nm are produced on silicon wafer substrates at room temperature by cosputtering $Fe_{50}Pt_{50}$ and Si_3N_4 targets. The adjustment of the power supplies of two separate dc and rf sputtering guns provides a wide range of effective insulator volume fractions of the thin film. The substrate is rotated at 75 rpm in order to attain uniform composition of the film.

The base pressure in the sputter chamber is 5×10^{-7} Torr. The sputtering pressure is fixed at 5 mTorr after introducing high purity argon gas (99.995%). The dc power source is set at 40 W, and rf power source is varied from 70 to 280 W for the sputtering guns, each of which is 2 in. in diameter. The deposition rate of FePt is about 0.3 nm/s. The as-deposited film is encapsulated in a quartz tube and then annealed in vacuum at various temperatures. The annealing time t_{an} is 30 min.

The magnetic properties of the film are measured with a vibrating sample magnetometer (VSM) and superconducting

a)Electronic mail: pckuo@ccms.ntu.edu.tw

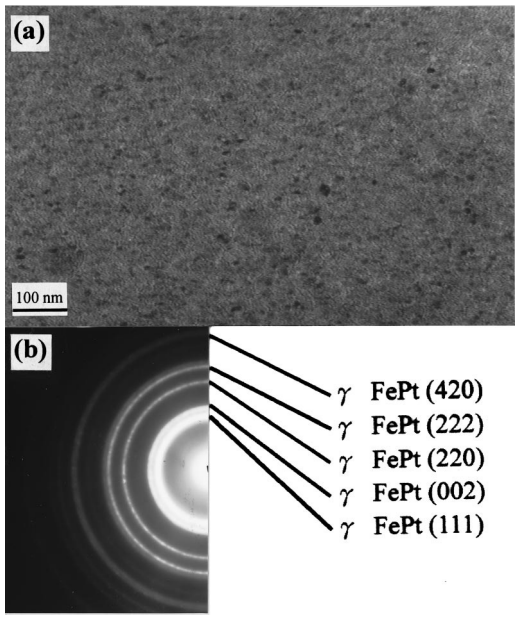

FIG. 1. TEM micrograph and electron diffraction pattern of the as-deposited $(FePt)_{80}-(Si_3N_4)_{20}$ film. (a) is the bright field image and (b) is the selected area diffraction (SAD) pattern of the FePt grains in (a).

quantum interference device (SQUID) at room temperature, with maximum applied fields are 13 and 50 kOe, respectively. The microstructure of the film is examined with a JOEL 100CX transmission electron microscope (TEM), and different phases of the film are identified by an x-ray diffractometer with Cu $K\alpha$ radiation. The average grain size of the film is measured from the TEM bright field image. Composition and homogeneity of the film are determined by energy disperse spectrum (EDS). The depth profiles of elements in the film are analyzed by Auger electron spectroscopy (AES) and the thickness of the film is measured by α step.

III. RESULTS AND DISCUSSION

From the TEM analysis, we find the microstructure of the as-deposited FePt–Si_3N_4 film is an amorphous Si_3N_4 matrix with γ-FePt grains dispersed in it. The average grain size of γ-FePt grains is about 5 nm for all as-deposited films. Figure 1 shows a typical example. Figure 1(a) is the TEM bright field image of the as-deposited $(FePt)_{80}-(Si_3N_4)_{20}$ film. The film thickness is 200 nm. The network-like structure results because the FePt grains are surrounded by a Si_3N_4 matrix. From selected area diffraction pattern analysis, we know that the crystal phase of the as-deposited film is a face-centered cubic (fcc) γ-FePt phase, as shown in Fig. 1(b). The well-marked diffraction rings indicates that the structure of the as-deposited film is not amorphous. As we compare this TEM diffraction pattern with that of the sputtered pure Si_3N_4 film, we confirm that the Si_3N_4 film has an amorphous structure in the as-deposition state.

The γ-FePt phase is soft magnetic in bulk form; however, due to the contribution of large internal stresses, it has higher coercivity in the thin film form than in the bulk form. These internal stresses may produce some microcracks in the as-deposited pure FePt film.[7] However, we find that these

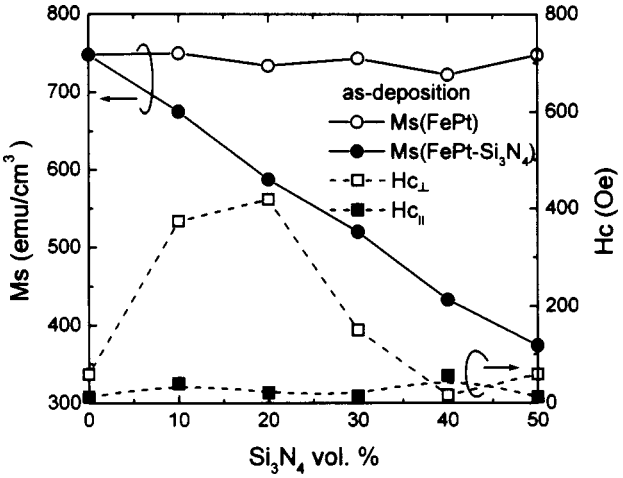

FIG. 2. Variations of *Ms* and *Hc* with Si_3N_4 volume fraction of various as-deposited FePt–Si_3N_4 films. Si_3N_4 volume fraction of the film is varied from 0 to 50 vol. %, and the film thickness is 200 nm.

microcracks disappear after the addition of Si_3N_4. This may be due to the fact that the internal stress of the film is released by the amorphous Si_3N_4 phase.

Figure 2 shows the relationships among saturation magnetization *Ms*, in-plane coercivity $Hc_{\parallel}$, perpendicular coercivity $Hc_{\perp}$, and Si_3N_4 volume fraction V_f of as-deposited FePt–Si_3N_4 films. We can see that the *Ms* value of the film is decreased linearly with increasing V_f, as shown in the line marked by solid dots. The *Ms* value is about 750 emu/cm^3 when V_f is 0 vol. %, and as V_f is increased to 50 vol. %, it decreases to about 375 emu/cm^3, which is only half of the pure FePt film. From this, it can be understood that Si_3N_4 is a nonmagnetic phase, and it plays only the simple role of diluting the magnetization of the film.

The *Ms* value of the line marked by circles in Fig. 2 is obtained by deducting the Si_3N_4 volume from the total film volume, so it reveals the intrinsic *Ms* of the magnetic $Fe_{50}Pt_{50}$ alloy. Note that this *Ms* value remains fairly constant with an increasing Si_3N_4 volume fraction. Since this *Ms* value does not vary with the Si_3N_4 volume fraction, means that Si_3N_4 is not reacting with Fe or/and Pt elements during the cosputtering process.

The variation of $Hc_{\parallel}$ with V_f is small, as V_f is between 0 and 50 vol. % Si_3N_4. $Hc_{\parallel}$ remains at about 50 Oe. However, the $Hc_{\perp}$ value of as-deposited film is increased with V_f from 60 to about 420 Oe as V_f increases from 0 to 20 vol. %; then it decreases with increasing V_f to about 20 Oe as V_f is increased to 40 vol. %. The $Hc_{\perp}$ value is always higher than $Hc_{\parallel}$ value for the as-deposited film, as V_f is lower than 35 vol. %. This may be due to the induced out of plane magnetic anisotropy by the internal stress. We can see that the addition of Si_3N_4 does not affect the intrinsic *Ms* of FePt alloy, but it will affect the extrinsic properties such as the coercivity. Since the average FePt grain size of all as-deposited films is almost the same, the variation of the coercivity with Si_3N_4 volume fraction is mainly due to the internal stress of the interface between Si_3N_4 and FePt phases which varies with Si_3N_4 volume fraction.

Figure 3 shows the x-ray diffraction patterns of the $(FePt)_{70}-(Si_3N_4)_{30}$ films, which are annealed at various tem-

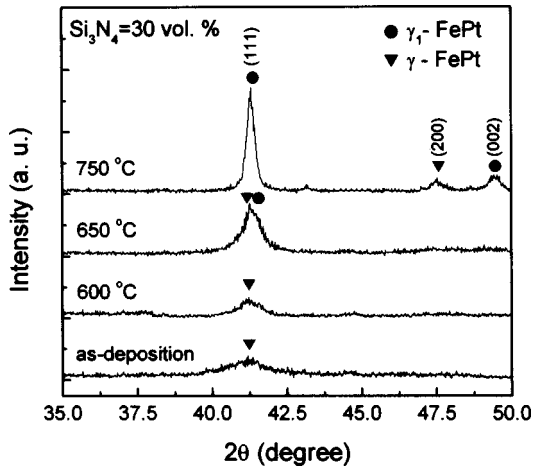

FIG. 3. X-ray diffraction patterns of various $(FePt)_{70}-(Si_3N_4)_{30}$ films. The film thickness is 200 nm and the film is ice-water quenched after annealing.

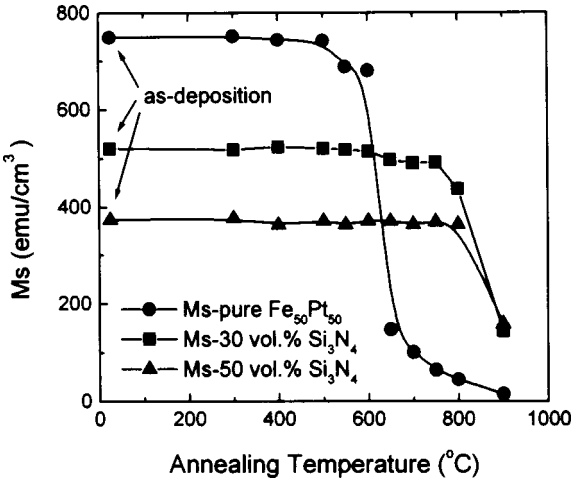

FIG. 4. Variations of the *Ms* with annealing temperature of various $FePt-Si_3N_4$ films. Si_3N_4 contents of the films are 0, 30, and 50 vol. %, respectively. The film thickness is 200 nm and the film is ice-water quenched after annealing.

peratures. For a pure FePt thin film, annealed at 600 °C for 30 min, we can find superlattice peaks in its x-ray diffraction pattern.[7] However, they cannot be found in the annealed $(FePt)_{70}-(Si_3N_4)_{30}$ granular film at this annealing temperature and time. In Fig. 3, we cannot see any well-marked superlattice peaks of γ_1-FePt phase, even at a higher annealing temperature (650 °C), because the amount of γ_1-FePt phase is very small at this annealing temperature. However, as the film is annealed at 750 °C, the superlattice peak of γ_1-FePt phase in this granular $(FePt)_{70}-(Si_3N_4)_{30}$ film is revealed. This is due to the fact that the γ-FePt phase is almost completely transformed to γ_1-FePt phase at this annealing temperature. This indicates that the addition of Si_3N_4 would increase the transformation temperature of γ-FePt to γ_1-FePt phase.

Table I listed $(FePt)_{100-x}-(Si_3N_4)_x$ $(x=20-50$ vol. %) thin films' (111) *d* spacings of γ-FePt phase and γ_1-FePt phase. The data of bulk $Fe_{50}Pt_{50}$ and two kinds of pure $Fe_{50}Pt_{50}$ thin films, which are ice-water quenched and furnace cooled after being annealed, are also included. We can see that the lattice parameter of FePt crystal decreased with increasing Si_3N_4 volume fraction. This may be due to fact that the sputtered FePt continuous alloy film has strong surface tension originally, and as Si_3N_4 isolated the FePt grains, the continuity of the alloy film is destroyed. This structure

TABLE I. Variations of *d* spacing with Si_3N_4 vol. %.

	As-deposition *d* value of (111) Å	750 °C postannealed *d* value of (111)s[c] Å
FePt (bulk)[a]	2.202[d]	2.197[d]
FePt (thin film)[a]	2.201	2.197
FePt (thin film)[b]	2.201	2.185
$(FePt)_{80}(Si_3N_4)_{20}$[a]	2.194	2.181
$(FePt)_{70}(Si_3N_4)_{30}$[a]	2.191	2.180
$(FePt)_{60}(Si_3N_4)_{40}$[a]	2.191	2.172
$(FePt)_{50}(Si_3N_4)_{50}$[a]	2.184	2.165

[a]Ice-water quenched.
[b]Furnace cooled.
[c]Superlattice.
[d]Refer to JCPDS (Joint Committee on Powder Diffraction Standards).

allowed the inner stress of the film to be released from the film body without the need to form microcracks to release the stress. However, the interface bonding between the FePt and Si_3N_4 phases have exerted compressive stress on the FePt grain and shortened its lattice parameter. Therefore, all *d* spacing of (111) planes of the as-deposited film and (111)*s* planes of the annealed film decrease with increasing Si_3N_4 volume fraction, as shown in Table I.

Figure 4 shows the relation between *Ms* and T_{an} of the annealed films with various Si_3N_4 volume fractions. We find that the *Ms* value of pure $Fe_{50}Pt_{50}$ alloy film is decreased quickly as T_{an} is increased to a temperature higher than 600 °C. This is due to the fact that FePt film reacts with the silicon substrate as $T_{an}>600$ °C.[8] However, when 30 or 50 vol. % Si_3N_4 is added, the *Ms* value of the film will decrease at $T_{an}>800$ °C, which is higher than that of pure FePt film.

Figure 4 implies that the Si_3N_4 phase in granular $FePt-Si_3N_4$ film protects the FePt phase at high temperatures, so the thermal stability of granular $FePt-Si_3N_4$ film is better than that of pure FePt film. For the films with 30 and 50 vol. % Si_3N_4, the abrupt decrease of *Ms* as $T_{an}>800$ °C is due to the interdiffusion of FePt with Si substrate. Figures 5(a) and 5(b) show the AES signals of the elements as a function of depth for $(FePt)_{70}-(Si_3N_4)_{30}$ films with (a) as-deposited, (b) $T_{an}=900$ °C, respectively. It is evident that both Fe and Pt atoms are diffused deeply into the Si substrate and reacted with Si atoms after being annealed at 900 °C. This reaction forms some compounds such as $FeSi_2$, Pt_6Si_5, etc., and are detected by x-ray analysis.

Figures 6(a) and 6(b) show the relationships among $Hc_{\parallel}$, $Hc_{\perp}$, and T_{an} of the annealed $FePt-Si_3N_4$ films with various Si_3N_4 volume fractions. As V_f is equal to 0 vol. % (i.e., pure $Fe_{50}Pt_{50}$), the $Hc_{\parallel}$ value can reach 10 kOe after the film is annealed at 600 °C. As T_{an} is higher than 650 °C, the $Hc_{\parallel}$ value of pure $Fe_{50}Pt_{50}$ film is lower than 2 kOe. The rapid decrease of $Hc_{\parallel}$ for $T_{an}>600$ °C is due to the grain growth and the reaction of FePt film with the silicon substrate. For the $(FePt)_{70}-(Si_3N_4)_{30}$ film, $Hc_{\parallel}$ value is about 2

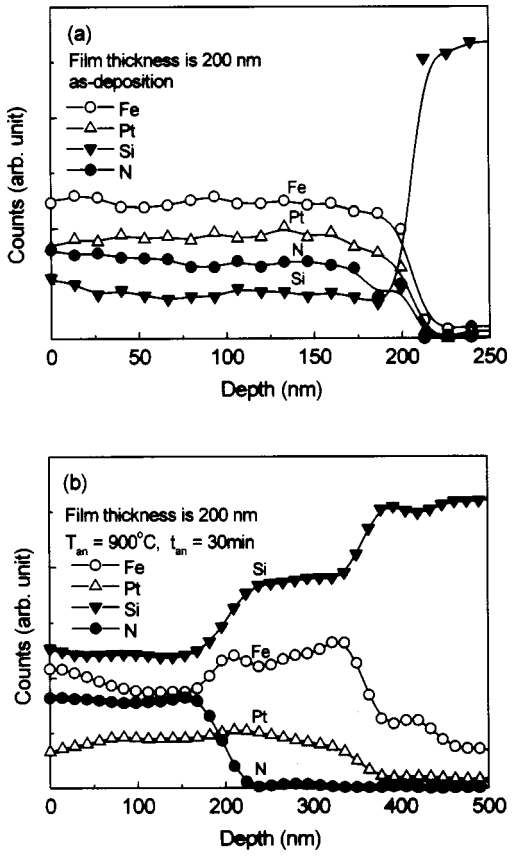

FIG. 5. AES depth profiles of the elements for the $(FePt)_{70}$–$(Si_3N_4)_{30}$ films with (a) as-deposited, (b) $T_{an}=900\,^{\circ}C$, respectively. The film thickness is 200 nm and the film (b) is ice-water quenched after annealing.

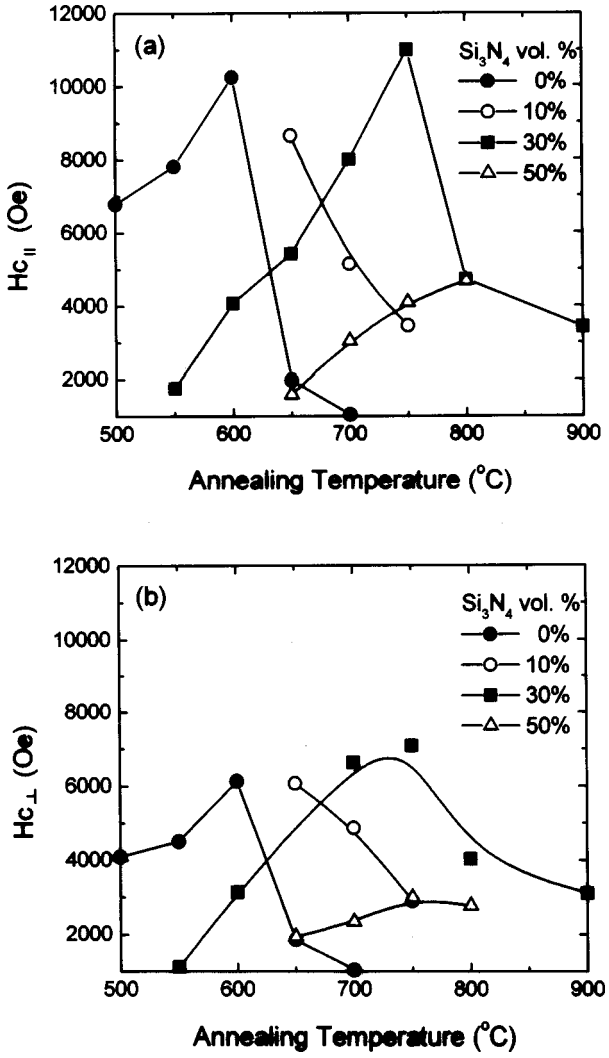

FIG. 6. Variations of $Hc_{\parallel}$ and $Hc_{\perp}$ with annealing temperature of various FePt–Si_3N_4 films; Si_3N_4 contents of the films are 0, 10, 30, and 50 vol. %, respectively. (a) $Hc_{\parallel}$ vs T_{an}, (b) $Hc_{\perp}$ vs T_{an}. The film thickness is 200 nm and the film is ice-water quenched after annealing.

kOe at $T_{an}=550\,^{\circ}C$, and it increases rapidly with increasing T_{an} to reach its maximum value of 11 kOe at $T_{an}=750\,^{\circ}C$ then decreases rapidly as T_{an} is increased further. In Fig. 4(b), $Hc_{\perp}$ value also has the same tendency as that of $Hc_{\parallel}$. The maximum $Hc_{\perp}$ value is about 7 kOe, which is much smaller than that of $Hc_{\parallel}$. Therefore, the magnetic anisotropy of this film is parallel to the film plane. The increase of $Hc_{\parallel}$ and $Hc_{\perp}$ values with increasing T_{an} as $T_{an}<750\,^{\circ}C$ is due to the gradual transformation of the soft γ-FePt phase to the hard γ_1-FePt phase, and the γ_1-FePt phase has very high magnetocrystalline anisotropy. As $T_{an}>750\,^{\circ}C$, the decrease of $Hc_{\parallel}$ and $Hc_{\perp}$ values with increasing T_{an} is also due to the growth of FePt grains and the reaction of FePt with the Si substrate. In general, $Hc_{\parallel}$ and $Hc_{\perp}$ values are increased with increasing T_{an} for annealed FePt–Si_3N_4 film, and will decrease after reaching their maximum values at some characteristic T_{an}.

From Fig. 6 we also can see that the increase of Si_3N_4 content in the film will increase the annealing temperature required for high coercivity. Pure $Fe_{50}Pt_{50}$ film must be annealed between 500 and 600 °C, resulting in a coercivity higher than 3 kOe, however, addition of 30 vol. % of Si_3N_4 raises this temperature range to between 600 and 900 °C. This is due to the fact that the amorphous Si_3N_4 phase postpones the initial temperature, which transforms the fcc γ-FePt phase to the fct γ_1-FePt phase.

For pure FePt film, the as-deposited γ-FePt thin film includes the nucleation site of γ_1-FePt phase. For the as-deposited FePt–Si_3N_4 film, the FePt particles are surrounded by the insulator Si_3N_4, which is a poor heat conductor. The γ-FePt particles in as-deposited FePt–Si_3N_4 film cannot be transformed to γ_1-FePt phase completely by quenching the film in ice water after annealing at 600 °C. The Si_3N_4 content would affect the magnetic hardness of the granular FePt–Si_3N_4 film after annealing.

From Fig. 6(a) we can see that the addition of the amorphous Si_3N_4 phase can raise the initial phase transformation temperature at which γ-FePt is transformed into the γ_1-FePt phase. The coercivity of annealed FePt–Si_3N_4 film could be larger than that of pure FePt film due to the completely isolated small FePt grains with appropriate intergranular distance and the stress anisotropy of the particles. As the amount of the magnetic phase is fixed, not only the magnetic grain size but also the intergranular distance are increased with increasing annealing temperature. The growth of mag-

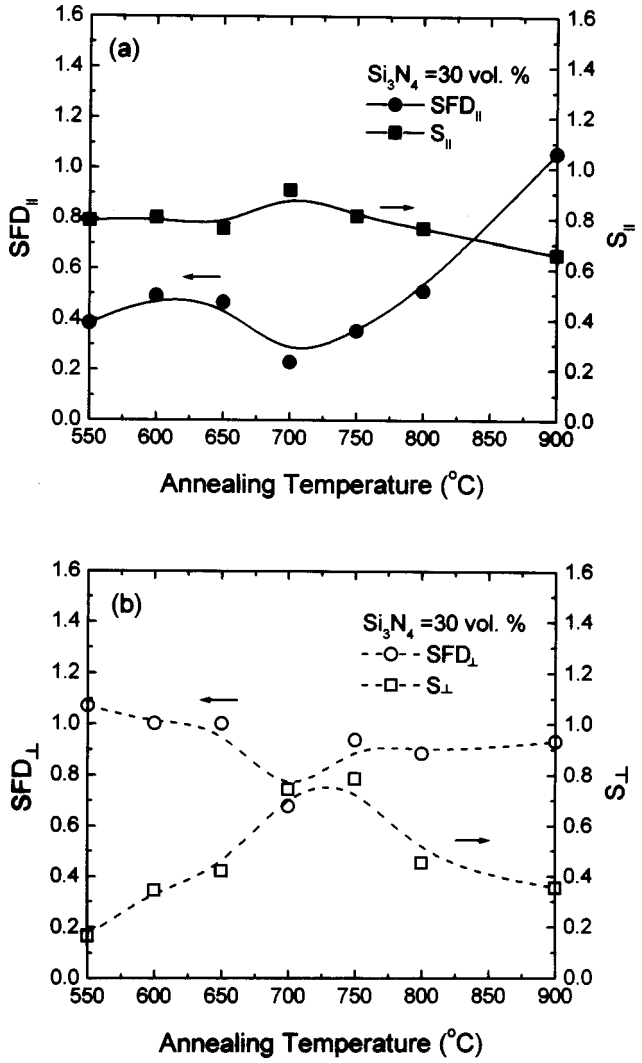

FIG. 7. Variations of squareness ($S=Mr/Ms$) and switching field distributions (SFD) with annealing temperature of the $(FePt)_{70}-(Si_3N_4)_{30}$ film. The film thickness is 200 nm and the film is ice-water quenched after annealing.

netic FePt grains would decrease the coercivity of granular film.

Figure 7(a) shows the relationships among in-plane squareness ($S_{\parallel}=Mr_{\parallel}/Ms$), switching field distribution ($SFD_{\parallel}$), and annealing temperature T_{an} of the $(FePt)_{70}-(Si_3N_4)_{30}$ film. We found that both the maximum $S_{\parallel}$ value and the minimum $SFD_{\parallel}$ value occur at $T_{an}\cong 700\,^{\circ}C$. The maximum $S_{\parallel}$ value is about 0.9, and the minimum $SFD_{\parallel}$ value is about 0.2. In Fig. 7(b), it is noticeable that the tendency of the $S_{\perp}$ vs T_{an} curve is similar to that of $S_{\parallel}$ vs T_{an} curve. The maximum $S_{\perp}$ value occurs at $T_{an}\cong 750\,^{\circ}C$; which is about 0.8. The minimum $SFD_{\perp}$ value is about 0.7, which is much larger than the minimum $SFD_{\parallel}$ value. In summary, the optimum annealing temperature for the in-plane magnetic properties of $(FePt)_{70}-(Si_3N_4)_{30}$ film is $T_{an}\cong 700\,^{\circ}C$. The *Ms* value, $Hc_{\parallel}$, and $Hc_{\perp}$ of this granular film at this annealing temperature are 530 emu/cm^3, 8 kOe, and 6.7 kOe, respectively.

Figures 8(a) and 8(b) are the TEM bright field image and electron diffraction pattern of the $(FePt)_{70}-(Si_3N_4)_{30}$ film, which is annealed at 750 °C. The thickness of the film is 200 nm. It is apparent that the spherical FePt grains are embedded in Si_3N_4 matrix, and they form a typical granular structure. Its average grain size is about 40 nm. Figure 8(b) reveals that the FePt grain of this film is fct γ_1-FePt phase. Additionally, when we have indexed the diffraction pattern's rings with JCPDS, it is confirmed that the Si_3N_4 phase still maintains an amorphous state after annealing at this temperature.

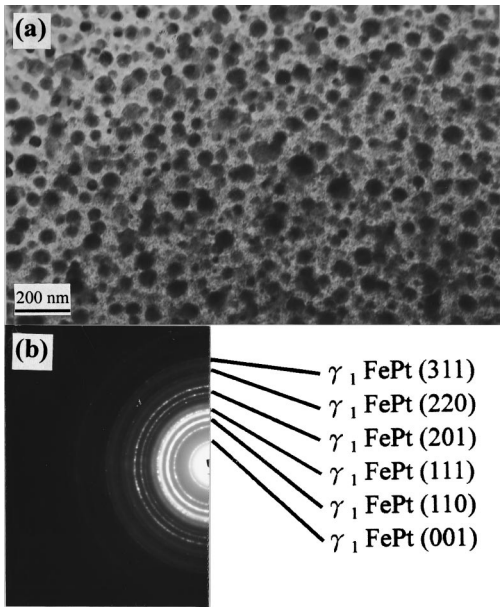

FIG. 8. TEM micrograph and electron diffraction pattern of the $(FePt)_{70}-(Si_3N_4)_{30}$ film which was annealed at 750 °C then ice-water quenched. (a) is the bright field image and (b) is the SAD pattern of the FePt grains in (a).

Figures 9(a) and 9(b) are the $M-H$ loops of the pure FePt film, are annealed at 600 °C, and the granular $(FePt)_{70}-(Si_3N_4)_{30}$ film, annealed at 750 °C, respectively. We can see that the *Ms* value of granular film ($Ms\cong 520$ emu/cm^3) is much lower than that of alloy film ($Ms\cong 780$ emu/cm^3). In fact, the *Ms* values of the magnetic phase in these two films are almost same. Due to the physical dilution of Si_3N_4, the *Ms* value of granular $(FePt)_{70}-(Si_3N_4)_{30}$ film is lower than that of pure FePt film.

The ''two shoulder'' shape of the $M-H$ loop of pure FePt film [see Fig. 9(a)] is reduced by adding Si_3N_4 phase, as shown in Fig. 9(b). The appearance of the two shoulder shape $M-H$ loop is due to the remnance of soft magnetic γ-FePt phase, which comes from incomplete transformation of γ-FePt$\rightarrow\gamma_1$-FePt phase. A pure γ_1-FePt phase will have a single $M-H$ loop without the two shoulder shape. It has been shown that the initial phase transformation temperature of granular $(FePt)_{70}-(Si_3N_4)_{30}$ film is higher than that of pure FePt film. Since the degree of γ-FePt$\rightarrow\gamma_1$-FePt phase transformation is increased with increasing the difference of supercooling temperatures ΔT at annealing treatment, the degree of γ-FePt$\rightarrow\gamma_1$-FePt phase transformation is more complete in granular $(FePt)_{70}-(Si_3N_4)_{30}$ film.

High coercivity of pure FePt film comes from both the high uniaxial magnetic crystalline anisotropy constant ($Ku\cong 7\times 10^7$ ergs/cm^3) of fct γ_1-FePt phase and the domain

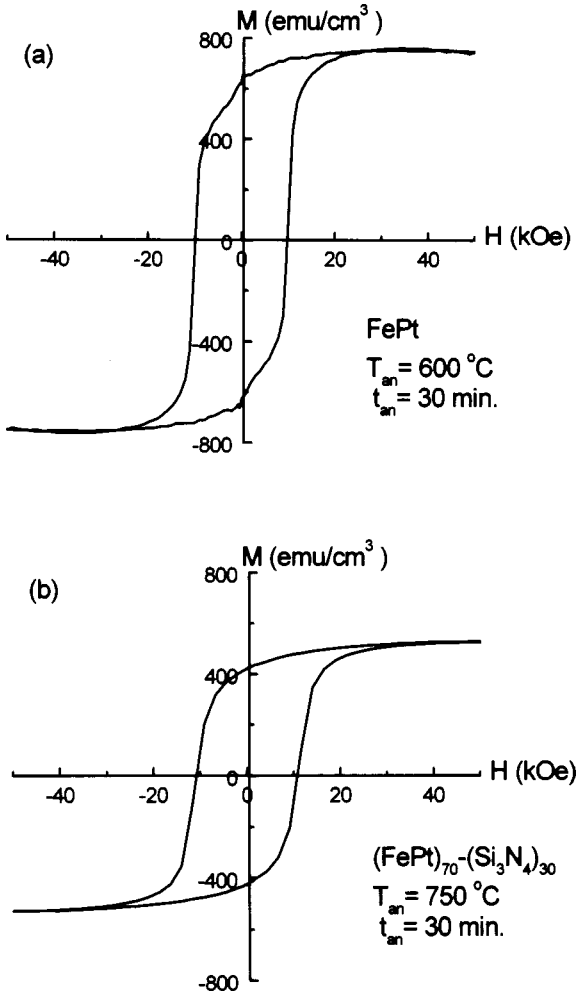

FIG. 9. (a) $M-H$ loop of the pure FePt film annealed at 600 °C. (b) $M-H$ loop of the granular $(FePt)_{70}-(Si_3N_4)_{30}$ film annealed at 750 °C. These films are ice-water quenched after annealing. The film thickness is 200 nm and the applied field is parallel to the film plane.

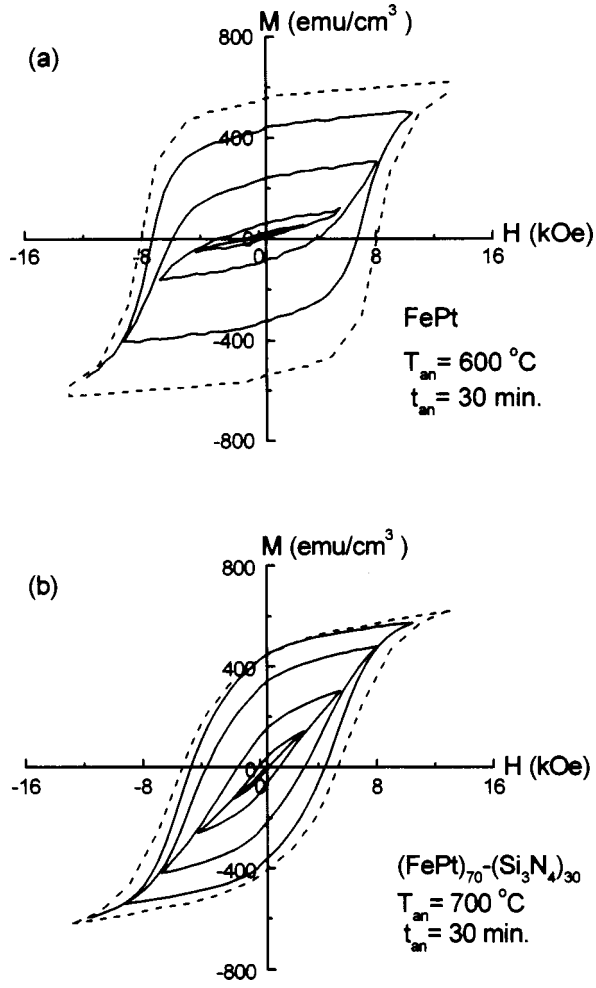

FIG. 10. (a) A series of minor loops of the pure FePt film annealed at 600 °C. (b) a series of minor loops of the $(FePt)_{70}-(Si_3N_4)_{30}$ film annealed at 700 °C. The film thickness is 200 nm and the film is ice-water quenched after annealing. The applied field is parallel to the film plane.

wall pinning effect of imperfect fct γ_1-FePt phase, as well.[9] According to Tanaka *et al.*,[10] antiphase boundaries and various orientations of γ_1-FePt twin's interfaces would be the pinning site that restrained domain wall motion. Figure 10(a) shows a series of minor loops of pure FePt film which are annealed at 600 °C and then quenched in ice water. It reveals an apparent domain wall pinning mechanism.

In granular FePt–Si_3N_4 film, it is impossible to attain nearly single γ_1-FePt phase under the same heat-treatment conditions as that of pure FePt alloy film. This is due to the fact that after annealing, the transfer of heat outside the film occurs more slowly as the volume fraction of Si_3N_4 phase is increased. The γ-FePt$\rightarrow\gamma_1$-FePt phase transformation could further be improved, when the film is annealed at higher temperature and quenched. But the crystal defects for pinning sites, such as antiphase boundaries and twins of fct γ_1-FePt phase will be decreased as T_{an} is increased.

Most of the FePt–Si_3N_4 films which are annealed at temperatures higher than the initial phase transformation temperature of γ-FePt$\rightarrow\gamma_1$-FePt cannot develop high coercivity because they have a greater amount of perfect fct γ_1-FePt phase, so the number of pinning sites is decreased. In the granular FePt–Si_3N_4 system, the surface of the FePt particle is strongly bonded with Si_3N_4 matrix, and the internal stress exists in the incoherent heterogeneous interface. Under a reversed magnetic field, domain nucleation may occur in the interface first, subsequently propagating to the whole particle. Therefore, the magnetic hardening mechanism of FePt–Si_3N_4 granular film is between domain wall nucleation and domain wall pinning. Figure 10(b) shows a series of minor loops of the $(FePt)_{70}-(Si_3N_4)_{30}$ film which is annealed at 700 °C and then quenched in ice water. It reveals a magnetic hardening mechanism between the domain wall nucleation type and the domain wall pinning type.

Figure 11 shows the relationship between the $Hc_{\parallel}$ of the minor loop and the applied field H_a of various annealed FePt–Si_3N_4 films. Solid lines show the data of granular films, and dashed lines show the data of pure FePt films. The $Hc_{\parallel}$ values are obtained from the minor loops of the VSM measurement, where the maximum H_a is 12 kOe. We can see that the pure FePt film quenched in ice water after being annealed exhibits the domain wall pinning mechanism, and the pure FePt film which was slowly cooled in a furnace

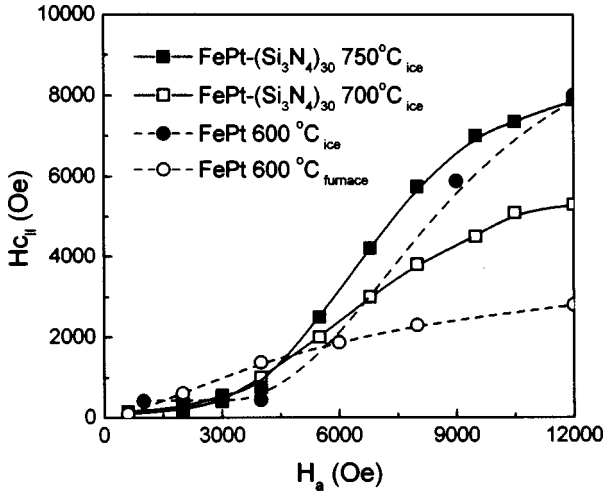

FIG. 11. $Hc_{\parallel}$ vs Ha of various annealed FePt and $(FePt)_{70}$–$(Si_3N_4)_{30}$ films. Solid lines are the $Hc_{\parallel}$ of the $(FePt)_{70}$–$(Si_3N_4)_{30}$ films which are quenched in ice water after annealing. Dashed lines are the $Hc_{\parallel}$ of the FePt films which are ice-water quenched and furnace cooled after annealing, respectively. These $Hc_{\parallel}$ values are obtained from VSM minor loops. The film thickness is 200 nm.

(cooling rate is about 4 °C/min) exhibits the domain nucleation mechanism.

In Fig. 11 we can see that when the applied field is below 6 kOe, $Hc_{\parallel}$ of the minor loop of granular $(FePt)_{70}$–$(Si_3N_4)_{30}$ film annealed at 750 °C and ice-water quenched is almost equal to that of pure FePt alloy film annealed at 600 °C and ice-water quenched. Comparing the $Hc_{\parallel}$ vs Ha curves of two $(FePt)_{70}$–$(Si_3N_4)_{30}$ granular films with that of ice-water-quenched pure FePt alloy film, the curves of these two $(FePt)_{70}$–$(Si_3N_4)_{30}$ granular films show that their magnetic hardening mechanism appear to be a mixture of domain nucleation and domain wall pinning.[11]

From the observations of TEM images, we find that the average grain size of FePt–Si_3N_4 composite film grows more slowly than that of pure FePt film when the annealing temperature is increased. Figure 12 shows the relationships among FePt grain size, V_f, and T_{an} of various FePt–Si_3N_4 films. The film thickness is 10 nm and the film is ice-water quenched after the annealing process. We can see that at the same T_{an}, the grain size of FePt in composite FePt–Si_3N_4 film is decreased as V_f is increased. This is due to the fact that the grain growth of magnetic FePt phase is limited by surrounding Si_3N_4 matrix in the FePt–Si_3N_4 composite film. As $T_{an}=750$ °C, the average grain size of pure FePt film is 90 nm, and it is only 70 nm in the $(FePt)_{70}$–$(Si_3N_4)_{30}$ film. The effect of Si_3N_4 addition is not only changing the film's magnetic hardening mechanism but also limiting the grain growth of magnetic FePt phase during annealing.

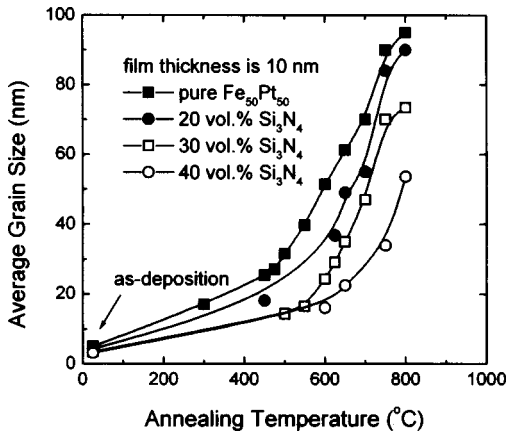

FIG. 12. Variations of FePt grain size with annealing temperature of various FePt–Si_3N_4 films. Si_3N_4 contents of the films are 0, 20, 30, and 40 vol. %, respectively. The film thickness is 10 nm and the film is ice-water quenched after annealing.

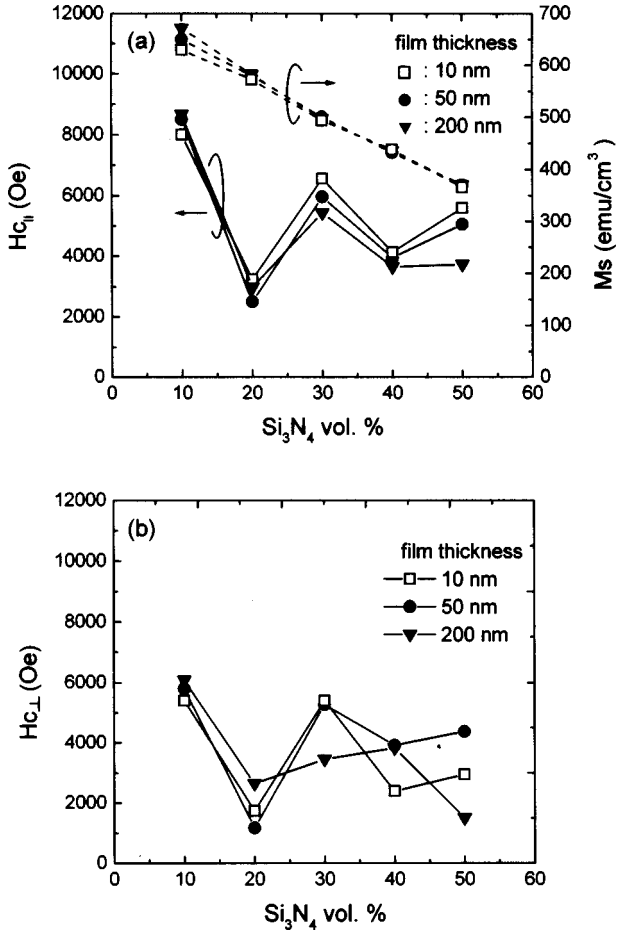

FIG. 13. (a) Variations of $Hc_{\parallel}$ and Ms with Si_3N_4 volume fraction, (b) relationships between $Hc_{\perp}$ and Si_3N_4 volume fraction of the annealed FePt–Si_3N_4 films. The film thicknesses are 10, 50, and 200 nm, respectively. The annealing temperature is 650 °C and the film is ice-water quenched after annealing.

Figure 13(a) shows the relationships among Ms, $Hc_{\parallel}$, and V_f of various granular FePt–Si_3N_4 films with film thickness of 10, 50, and 200 nm, respectively. It can be seen that the Ms value is independent of the film thickness but decreases linearly with increasing V_f. The dependence of the $Hc_{\parallel}$ value on film thickness is small. However, $Hc_{\parallel}$ varies with V_f as a sinusoidal curve. The amplitude of this sinusoidal curve is decreased as V_f is increased.

Figure 13(b) shows the variation of $Hc_{\perp}$ with film thickness and V_f. Except for the 200-nm-thick film, the variations of $Hc_{\perp}$ with V_f for the 10- and 50-nm-thick films also have the same tendency as that of $Hc_{\parallel}$, but their $Hc_{\perp}$ values are

much smaller than those of $Hc_{\parallel}$ for the same V_f. The variation of $Hc_{\parallel}$ and $Hc_{\perp}$ with V_f is irregular. This may be due to the fact that the particle size of FePt is decreased with increasing V_f (see Fig. 12) and the stress anisotropy of FePt particles is varied with V_f. In the granular FePt–Si_3N_4 system, the *Ms* value of FePt is not affected by the addition of Si_3N_4 since the insulator Si_3N_4 has not been alloyed with the magnetic FePt phase. Due to the *Ms* value of FePt in granular FePt–Si_3N_4 system remains constant, the effective magnetic anisotropy constant *K* of the FePt particle is dependent on its grain size and stress.

IV. CONCLUSIONS

We have investigated the magnetic properties and microstructure of cosputtered composite $(FePt)_{100-x}-(Si_3N_4)_x$ ($x = 0-50$ vol. %) films over a variety of annealing temperatures and film thicknesses. The *Ms* value of the film decreased linearly with increasing Si_3N_4 content. Granular FePt–Si_3N_4 films with high magnetic anisotropy FePt nanoparticles embedded in amorphous Si_3N_4 matrix can be obtained by annealing the film at suitable temperatures. The dependence of coercivity on film thickness is small. The average particle size of FePt particles in the FePt–Si_3N_4 film increased with increasing annealing temperature but decreased with increasing Si_3N_4 content. Varying the annealing temperature and Si_3N_4 volume fraction can control coercivity of the FePt–Si_3N_4 film and particle size of FePt particles. Maximum in-plane coercivity of the FePt–Si_3N_4 film is 11 kOe, a point which occurs at 30 vol. % of Si_3N_4 with the film being annealed at 750 °C and subsequently ice-water quenched. The analysis of the transmission electron microscopy diffraction pattern indicates that the crystalline phase of this granular film is nearly single γ_1-FePt phase with fct structure. The average grain size of the FePt particles in this film is about 40 nm.

ACKNOWLEDGMENT

This work was supported by the National Science Council of ROC through Grant No. NSC 88-2216-E-002-032.

[1] J.-G. Zhu, IEEE Trans. Magn. **MAG-29**, 195 (1993).
[2] S. H. Liou and C. L. Chien, J. Appl. Phys. **63**, 4240 (1988).
[3] S. M. Han, S. C. Yu, W. T. Kim, S. H. Han, and H. J. Kim, IEEE Trans. Magn. **MAG-33**, 3610 (1997).
[4] I. Kaitsu, A. Inomata, I. Okamoto, and M. Shinohara, IEEE Trans. Magn. **MAG-34**, 1591 (1998).
[5] J. N. Zhou, A. Butera, H. Jiang, and J. A. Barnard, J. Appl. Phys. **84**, 5693 (1998).
[6] M. Watanabe, T. Nakayama, K. Watanabe, T. Hirayama, and A. Tonomura, Mater. Trans., JIM **37**, 489 (1996).
[7] C.-M. Kuo, P. C. Kuo, and H.-C. Wu, J. Appl. Phys. **85**, 2264 (1999).
[8] C.-M. Kuo, P. C. Kuo, and H.-C. Wu, Y. D. Yao, and C. H. Lin, J. Appl. Phys. **85**, 4886 (1999).
[9] K. Watanabe, Mater. Trans., JIM **29**, 80 (1988).
[10] Y. Tanaka, N. Kimura, K. Hono, K. Yasuda, and T. Sakurai, J. Magn. Magn. Mater. **170**, 289 (1997).
[11] G. C. Hadjipaanayis and A. Kim, J. Appl. Phys. **63**, 3310 (1988).